In vivo mouse myocardial P-31 MRS using three-dimensional image-selected in vivo spectroscopy (3D ISIS): technical considerations and biochemical validations

Research article

NMR IN BIOMEDICINE

Received: 17 May 2015, Revised: 24 June 2015, Accepted: 9 July 2015, Published online in Wiley Online Library: 13 August 2015

(wileyonlinelibrary.com) DOI: 10.1002/nbm.3371

In vivo mouse myocardial ^{31}P MRS using three-dimensional image-selected *in vivo* spectroscopy (3D ISIS): technical considerations and biochemical validations

Adrianus J. Bakermans[a,b]*†, Desiree Abdurrachim[a†], Bastiaan J. van Nierop[a], Anneke Koeman[c], Inge van der Kroon[a], Antonius Baartscheer[d], Cees A. Schumacher[d], Gustav J. Strijkers[a,e], Sander M. Houten[f], Coert J. Zuurbier[c], Klaas Nicolay[a] and Jeanine J. Prompers[a]

^{31}P MRS provides a unique non-invasive window into myocardial energy homeostasis. Mouse models of cardiac disease are widely used in preclinical studies, but the application of ^{31}P MRS in the *in vivo* mouse heart has been limited. The small-sized, fast-beating mouse heart imposes challenges regarding localized signal acquisition devoid of contamination with signal originating from surrounding tissues. Here, we report the implementation and validation of three-dimensional image-selected *in vivo* spectroscopy (3D ISIS) for localized ^{31}P MRS of the *in vivo* mouse heart at 9.4 T. Cardiac ^{31}P MR spectra were acquired *in vivo* in healthy mice (n = 9) and in transverse aortic constricted (TAC) mice (n = 8) using respiratory-gated, cardiac-triggered 3D ISIS. Localization and potential signal contamination were assessed with ^{31}P MRS experiments in the anterior myocardial wall, liver, skeletal muscle and blood. For healthy hearts, results were validated against *ex vivo* biochemical assays. Effects of isoflurane anesthesia were assessed by measuring *in vivo* hemodynamics and blood gases. The myocardial energy status, assessed via the phosphocreatine (PCr) to adenosine 5′-triphosphate (ATP) ratio, was approximately 25% lower in TAC mice compared with controls (0.76 ± 0.13 *versus* 1.00 ± 0.15; $P < 0.01$). Localization with one-dimensional (1D) ISIS resulted in two-fold higher PCr/ATP ratios than measured with 3D ISIS, because of the high PCr levels of chest skeletal muscle that contaminate the 1D ISIS measurements. *Ex vivo* determinations of the myocardial PCr/ATP ratio (0.94 ± 0.24; n = 8) confirmed the *in vivo* observations in control mice. Heart rate (497 ± 76 beats/min), mean arterial pressure (90 ± 3.3 mmHg) and blood oxygen saturation (96.2 ± 0.6%) during the experimental conditions of *in vivo* ^{31}P MRS were within the normal physiological range. Our results show that respiratory-gated, cardiac-triggered 3D ISIS allows for non-invasive assessments of *in vivo* mouse myocardial energy homeostasis with ^{31}P MRS under physiological conditions. Copyright © 2015 John Wiley & Sons, Ltd.

Keywords: energy metabolism; heart; ISIS; mouse; ^{31}P MRS; transverse aortic constriction (TAC)

* *Correspondence to: A. J. Bakermans, Department of Radiology (Z0-180), Academic Medical Center, University of Amsterdam, Meibergdreef 9, 1105 AZ Amsterdam, the Netherlands.*
E-mail: a.j.bakermans@amc.uva.nl

a *A. J. Bakermans, D. Abdurrachim, B. J. van Nierop, I. van der Kroon, G. J. Strijkers, K. Nicolay, J. J. Prompers*
Biomedical NMR, Department of Biomedical Engineering, Eindhoven University of Technology, Eindhoven, the Netherlands

b *A. J. Bakermans*
Department of Radiology, Academic Medical Center, University of Amsterdam, Amsterdam, the Netherlands

c *A. Koeman, C. J. Zuurbier*
Laboratory of Experimental Intensive Care and Anesthesiology, Department of Anesthesiology, Academic Medical Center, University of Amsterdam, Amsterdam, the Netherlands

d *A. Baartscheer, C. A. Schumacher*
Experimental Cardiology, Heart Failure Research Center, Academic Medical Center, University of Amsterdam, Amsterdam, the Netherlands

e *G. J. Strijkers*
Biomedical Engineering and Physics, Academic Medical Center, University of Amsterdam, Amsterdam, the Netherlands

f *S. M. Houten*
Laboratory Genetic Metabolic Diseases, Department of Clinical Chemistry, and Department of Pediatrics, Emma Children's Hospital, Academic Medical Center, University of Amsterdam, Amsterdam, the Netherlands

† *These authors contributed equally to this work.*

Abbreviations used: *1D, 2D, 3D, one-, two-, three-dimensional; α-, β-, γ-ATP, α-, β-, γ-phosphate groups in adenosine 5′-triphosphate; CSI, chemical shift imaging; 2,3-DPG, 2,3-diphosphoglycerate; ECG, electrocardiogram; EDTA, ethylenediaminetetraacetic acid; EDV, end-diastolic volume; EF, ejection fraction; ESV, end-systolic volume; ISIS, image-selected in vivo spectroscopy; LV, left ventricle/left ventricular; LW, line width; MAP, mean arterial pressure; NA, number of averages; PCr, phosphocreatine; PDE, phosphodiesters; P_i, inorganic phosphate; SD, standard deviation; SNR, signal-to-noise ratio; SV, stroke volume; TAC, transverse aortic constriction/transverse aortic constricted.*

INTRODUCTION

Mouse models are widely used in preclinical studies on the pathogenesis of cardiomyopathies. Disturbed myocardial energy metabolism has been identified as an important contributor to the development of cardiomyopathy (1). The assessment of the myocardial energy status is therefore instrumental in the characterization of disease progression or treatment response. The high-energy phosphates adenosine 5′-triphosphate (ATP) and phosphocreatine (PCr) are essential for providing energy for cellular processes, such as sarcomere contraction in cardiomyocytes, and for energy transport and buffering. The inherent instability of high-energy phosphates compromises the accurate assessment of the myocardial energy status with biochemical techniques, which require disruptive or terminal biopsies, precluding longitudinal *in vivo* investigations. Many MRI and, to a lesser extent, MRS methods have been introduced to study the *in vivo* mouse heart non-invasively (2–4). These methods allow for longitudinal studies of disease progression and assessments of the effects of therapeutic strategies.

^{31}P MRS is the only method that provides a non-invasive window into *in vivo* high-energy phosphates (1). Localized signal acquisition is essential to restrict the spectrum obtained to the heart, excluding signal from nearby liver tissue or chest skeletal muscle. Localization methods for ^{31}P MRS include single-voxel as well as chemical shift imaging (CSI) approaches. ^{31}P CSI allows for an assessment of regional differences in myocardial energy status (5), but is susceptible to intervoxel signal contamination as a result of Fourier bleeding (6). In contrast, single-voxel localization with three-dimensional image-selected *in vivo* spectroscopy (3D ISIS) (7) leads to a better defined voxel shape (8), but the voxel size is typically much larger compared with CSI, and commonly includes the whole left ventricle (LV) (9).

Localized ^{31}P MRS of the *in vivo* mouse heart is very challenging because of the small organ size (~100 mg), high heart rate (~500 beats/min) and intrinsically low sensitivity of ^{31}P MRS. Methods for *in vivo* one-dimensional (1D) and two-dimensional (2D) ^{31}P CSI of the mouse heart were initially demonstrated in healthy mice (10) and in a transgenic mouse model for cardiomyopathy (11). These experiments were performed at a constant TR, which is essential for reliable signal quantification. None of these methods used cardiac triggering or respiratory gating to account for physiological motion of the tissue of interest. Together with the effects of Fourier bleeding in CSI methods, tissue displacement could lead to contamination of the spectrum with signal from the liver, blood and/or chest skeletal muscle.

One early study describes the application of cardiac-triggered 3D ISIS for *in vivo* ^{31}P MRS of the mouse heart (9). Although cardiac triggering was used in these experiments to synchronize the acquisitions with the cardiac cycle, no measures were taken to ensure a constant TR. When applying ISIS under partially saturated conditions (i.e. if TR $< 5 \times T_1$), variations in TR can lead to signal contamination (12,13), as well as modulations of signal amplitudes, as a result of T_1-dependent partial saturation effects. These early experiments were performed at 2.35 T and required a lengthy experimental time of nearly 3 h (9). At higher field strengths, the scan time can possibly be reduced to acceptable values whilst maintaining sufficient signal-to-noise ratio (SNR) for signal quantification.

Here, we report the implementation of 3D ISIS for single-voxel localized ^{31}P MRS of the *in vivo* mouse heart at 9.4 T. Because 3D ISIS is a multi-shot localization method, and hence particularly sensitive to motion artifacts, we employed both respiratory gating and cardiac triggering whilst maintaining a steady state of magnetization with dummy excitations during respiratory gates to ensure a constant TR (14). Results were validated against *ex vivo* biochemical assays of myocardial PCr and ATP concentrations. Hemodynamics and blood gases were measured to assess the potential effects of isoflurane anesthesia on the cardiovascular physiology. To demonstrate suitability for cardiac applications, the method was applied to a well-characterized mouse model of heart failure (15,16).

METHODS

Animals

All procedures were approved by the Animal Ethics Committee of Maastricht University (Maastricht, the Netherlands). Male C57BL/6 mice ($n = 8$; body weight, 26.2 ± 2.6 g) underwent transverse aortic constriction (TAC) surgery as described previously (17). Anesthesia was induced using 2–3% isoflurane in a 0.4-L/min flow of 1 : 1 O_2 : medical air, after which mice were intubated for mechanical ventilation. Analgesia was provided using buprenorphine (0.1 mg/kg, subcutaneous). An incision was made above the first intercostal space to gain access to the aortic arch. The aorta was tied off with a 27G needle between the innominate artery and the left common carotid artery with a 6-0 silk suture. Subsequent needle removal left an aortic stenosis, inducing LV pressure overload. The chest was closed and the intubation tube was removed to allow full recovery. Seven weeks after surgery, MR data were acquired as described below. Healthy mice ($n = 9$; body weight, 24.4 ± 2.0 g) served as controls. Following the MR measurements, anesthetized mice were sacrificed by exsanguination. Blood was collected in ethylenediaminetetraacetic acid (EDTA) tubes for *ex vivo* analysis with ^{31}P MRS.

MR protocol

Mice were anesthetized with 2–3% isoflurane in a 0.4-L/min flow of medical air and positioned prone in a purpose-built support cradle above a custom-built, actively decoupled, two-turn ^{31}P surface coil (Ø = 15 mm) for signal reception. Anesthesia was maintained with 1.2–1.6% isoflurane in a continuous flow of 0.4 L/min of medical air. The front paws were taped onto gold-coated electrocardiogram (ECG) electrodes integrated in the anesthesia mask. A respiratory balloon was positioned underneath the lower abdomen. Vital signs were monitored and used for MR gating and triggering by the SA Monitoring and Gating System 1025 (Small Animal Instruments, Stony Brook, NY, USA). Mouse body temperature was maintained using a heating pad with integrated warm water flow, and monitored with an external abdominal fiber-optic probe. The set-up was inserted into a horizontal-bore 9.4-T magnet (Magnex Scientific, Yarnton, Oxford, UK), interfaced to a Bruker Avance III console (Bruker Biospin MRI, Ettlingen, Germany) and controlled by the ParaVision 5.0 software package (Bruker Biospin). The system was equipped with a 740-mT/m gradient set and a volume coil (Ø = 54 mm) composed of a quadrature ^{1}H birdcage resonator and a linear ^{31}P birdcage resonator (RAPID Biomedical, Rimpar, Germany), used for ^{1}H MRI and shimming, and for radiofrequency transmission for ^{31}P MRS, respectively.

Scout ^{1}H MR images were acquired to confirm the positioning of the heart within the sensitive area of the ^{31}P surface coil. A segmented, prospectively cardiac-triggered, respiratory-gated, fast low-angle shot sequence was used to acquire a cine ^{1}H MR image series of 16–18 frames per cardiac cycle. Four 1-mm LV short-axis slices were complemented with four- and two-chamber long-axis views, and used for the quantification of LV function and morphology, as well as for anatomical reference during 3D ISIS voxel planning for localized ^{31}P MRS. The imaging parameters were as follows: field of view, 30 × 30 mm^2; matrix, 128 × 128; TE = 1.8 ms; TR = 7 ms; flip angle, 15°; number of averages (NA) = 4. The total acquisition time was approximately 20 min.

Subsequently, an 11 × 11 × 11-mm^3 voxel in the sensitive area of the surface coil was shimmed manually by minimization of the $^{1}H_2O$ line width (LW), acquired with a respiratory-gated, cardiac-triggered, point-resolved spectroscopy sequence (18). Calibration of the ^{31}P sinc excitation pulse (pulse length, 1.2 ms; bandwidth, 32.0 ppm) was performed by varying the pulse power to achieve the maximal signal from a spherical phantom (Ø = 5 mm; 15 M phosphoric acid) positioned underneath the ^{31}P surface coil. After removal of the phantom, unlocalized pulse-acquire ^{31}P MR spectra were obtained from a subset of animals (n = 5 per group) to assess metabolite T_1 values using conventional saturation recovery experiments. The parameters were as follows: 1.2-ms 90° sinc excitation pulse; bandwidth, 32.0 ppm; γ-ATP on resonance; TR = 500, 1000, 2000, 4000, 6000 and 15 000 ms; NA = 1024–32.

Next, a respiratory-gated, cardiac-triggered 3D ISIS sequence was used for localized cardiac ^{31}P MRS. Dependent on heart size, a 3D ISIS voxel (TAC: 326 ± 43 μL *versus* control: 175 ± 8.8 μL) was positioned to enclose the end-diastolic LV, carefully excluding the liver and chest skeletal muscle (Fig. 1A, B). The 3D ISIS parameters were as follows: TR ≈ 2 s; NA = 768 (96 3D ISIS cycles) preceded by one dummy cycle; 6.25-ms 180° adiabatic hyperbolic secant inversion pulses (bandwidth, 37.5 ppm); 1.2-ms 90° sinc excitation pulse (bandwidth, 32.0 ppm); γ-ATP on resonance; 2048 acquisition points. Although the excitation pulse was calibrated, the potential effect of spatial contamination by so-called 'T_1 smearing' as a result of inhomogeneous excitation pulses (19) was further minimized by choosing the least-optimal inversion order in the left–right orientation. This avoided contamination of the spectra with signal from chest skeletal muscle (anterior–posterior orientation) or the liver (head–feet orientation). Triggering was timed at ECG R-wave upslope detection. Respiratory gating causes fluctuations in effective TR, leading to variations in longitudinal magnetization between subsequent acquisitions. If longitudinal magnetization is not equal at the start of all eight acquisitions within one 3D ISIS cycle, the cancellation of unwanted signals in the addition/subtraction scheme is incomplete. Thus, when measuring at TR < 5 × T_1, a constant TR is required to minimize signal contamination. Moreover, measurement at constant TR prevents complex modulations of signal amplitudes that hamper corrections for partial saturation effects. Therefore, we performed unlocalized dummy excitation pulses during respiratory gates to achieve an essentially constant TR of 2 s. The acquisition time was less than 40 min. In a subset of healthy mice (n = 6), 3D ISIS was also performed at TR ≈ 15 s; NA = 192 (24 cycles). These measurements were used to verify the partial saturation correction factor obtained with unlocalized saturation recovery experiments.

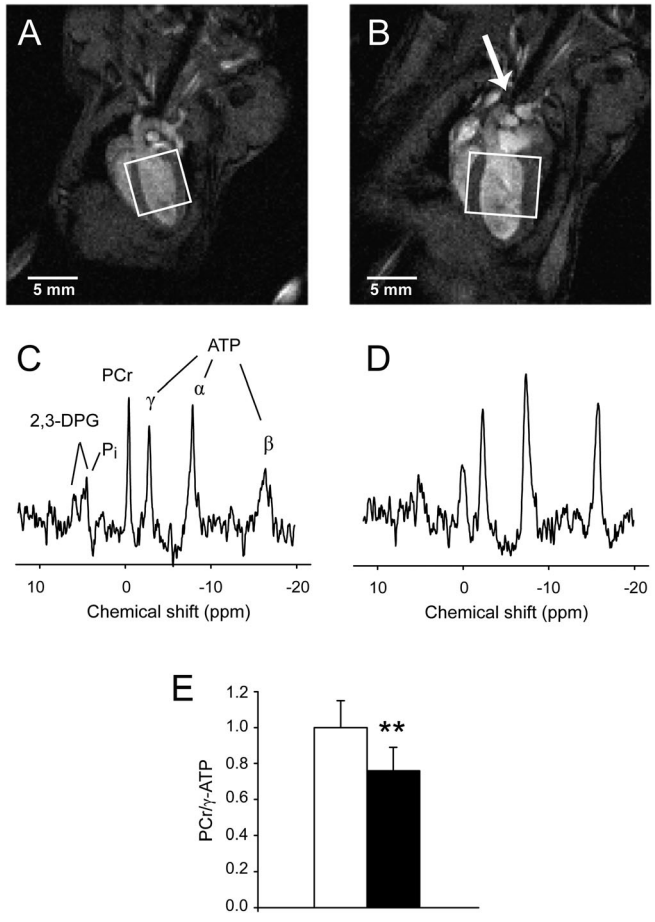

Figure 1. End-diastolic left ventricular (LV) MR images obtained from a control mouse (A) and a mouse with a transverse aortic constriction (TAC) (B). The constriction is indicated by the arrow. Dilated hypertrophic cardiomyopathy is evidenced by increased LV wall thickness and LV cavity volume in the TAC mouse. Rectangles indicate the voxels selected for localized ^{31}P MRS with three-dimensional image-selected *in vivo* spectroscopy (3D ISIS). (C, D) ^{31}P MR spectra acquired *in vivo* with 3D ISIS in a healthy mouse heart and a TAC heart, respectively. Myocardial PCr/γ-ATP, corrected for partial saturation, was lower in TAC mice (n = 8) compared with healthy controls (n = 9) (E). Data are expressed as mean ± standard deviation (SD). $^{**}P < 0.01$. α-, β-, γ-ATP, α-, β- and γ-phosphate groups in adenosine 5′-triphosphate; 2,3-DPG, 2,3-diphosphoglycerate; PCr, phosphocreatine; P_i, inorganic phosphate.

To compare 3D ISIS localization with 1D localization, we acquired spectra using 1D ISIS of the anterior myocardial wall in a slice essentially parallel to the surface coil (Fig. 2A) in a subset of mice (n = 6). Acquisition parameters were kept similar to the 3D ISIS approach, except for NA = 384 (192 1D ISIS cycles) and a slice thickness of 1 mm. Furthermore, to obtain spectra solely from the myocardium and to rule out any contamination with signal from LV cavity blood, 3D ISIS was performed with a small voxel (1 × 3 × 3 mm^3) positioned within the anterior myocardial wall (Fig. 2B). The acquisition time was approximately 2.5 h with NA = 3072 (384 cycles).

In addition, spectra from the liver and hind limb skeletal muscle (n = 3) were acquired *in vivo* with respiratory-gated and cardiac-triggered 3D ISIS (Fig. 3) to evaluate the performance of 3D ISIS localization with respect to *in vivo* ^{31}P MRS of these tissues, as reported in the literature (20,21).

Finally, to investigate the contribution of blood metabolites to the cardiac ^{31}P MR spectra acquired *in vivo*, spectra of fresh blood were measured *ex vivo* using a pulse-acquire sequence.

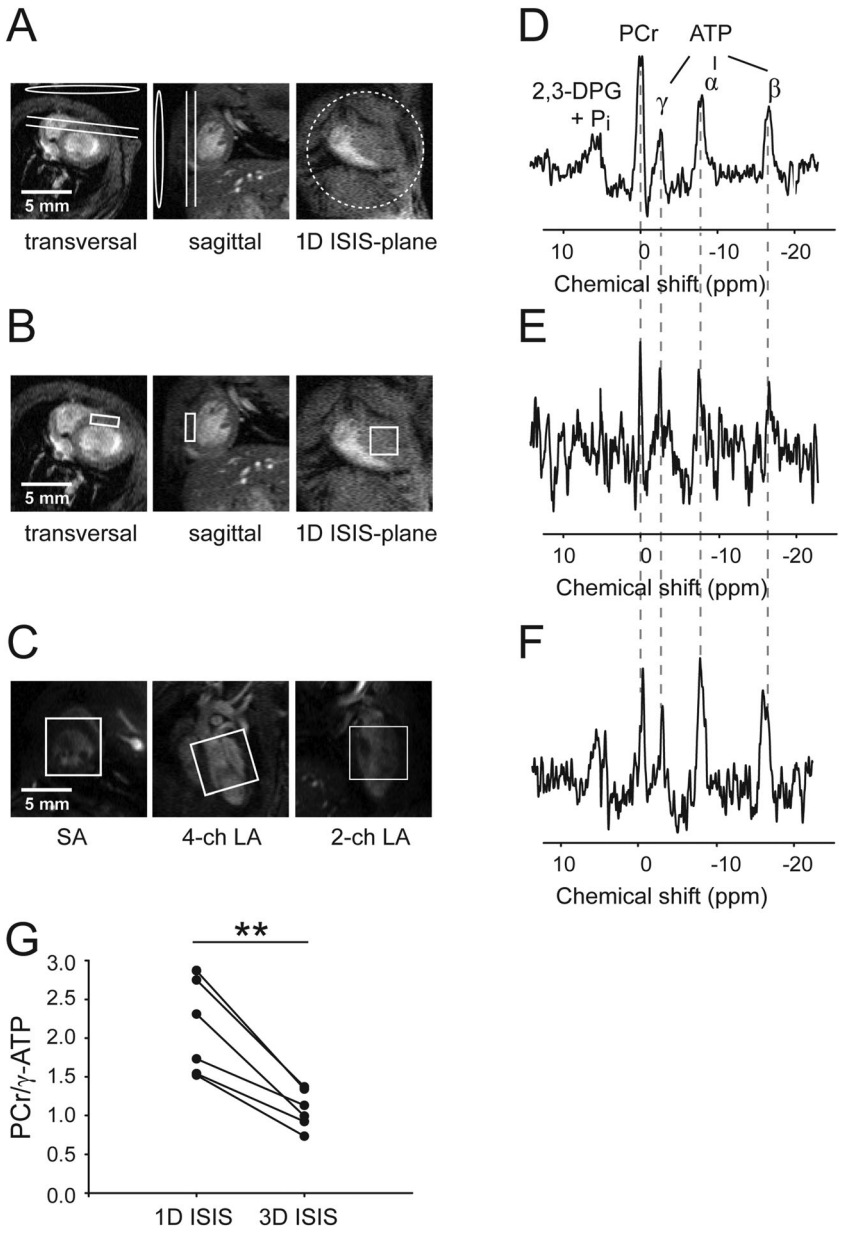

Figure 2. Comparisons of one-dimensional image-selected *in vivo* spectroscopy (1D ISIS) and three-dimensional image-selected *in vivo* spectroscopy (3D ISIS) localization for cardiac ^{31}P MRS. Geometrical localization for: (A) 1D ISIS in the anterior myocardial wall (slice thickness, 1 mm), indicated in transversal and sagittal reference images. Circle and ellipses indicate the position of the ^{31}P surface coil. 3D ISIS voxel localization in: (B) the anterior myocardial wall ($1 \times 3 \times 3$ mm^3) and (C) enclosing the whole left ventricle (LV) ($6 \times 6 \times 6$ mm^3). The corresponding ^{31}P MR spectra from: (D) 1D ISIS (NA = 384), (E) 3D ISIS in the myocardium (NA = 3072) and (F) 3D ISIS of the whole LV (NA = 384). All spectra were acquired in the same mouse at TR = 2 s. (G) PCr/γ-ATP ratio assessed via 1D ISIS (as in A) and 3D ISIS of the whole LV (as in C). $^{**}P < 0.01$ (two-sided paired *t*-test, $n = 6$). α-, β-, γ-ATP, α-, β- and γ-phosphate groups in adenosine 5′-triphosphate; 2-ch LA, two-chamber long axis; 4-ch LA, four-chamber long axis; 2,3-DPG, 2,3-diphosphoglycerate; NA, number of averages; PCr, phosphocreatine; P_i, inorganic phosphate. SA, short axis.

A vial ($n = 6$) with approximately 1 mL of blood in EDTA was positioned just over the surface coil and maintained at 37 °C by a heating pad. The parameters were as follows: 1.2-ms 90° sinc excitation pulse; γ-ATP on resonance; TR = 2000 ms; NA = 512.

Image analysis

LV cavity and myocardial wall volumes were quantified by semi-automatic segmentation of the cine images (Pie Medical Imaging, Maastricht, the Netherlands), as described previously (22), yielding LV end-diastolic volume (EDV), end-systolic volume (ESV), stroke volume (SV), ejection fraction (EF) and LV myocardial mass.

^{31}P MRS data analysis

Fitting of the metabolite signals to Lorentzian line shapes was performed in the time domain using AMARES in jMRUI (23). The PCr resonance was used as an internal chemical shift reference at 0.00 ppm. The ATP resonances at −2.48 ppm (γ; doublet), −7.52 ppm (α; doublet) and −16.26 (β; triplet) were fitted with equal amplitudes and LWs within each multiplet, and a

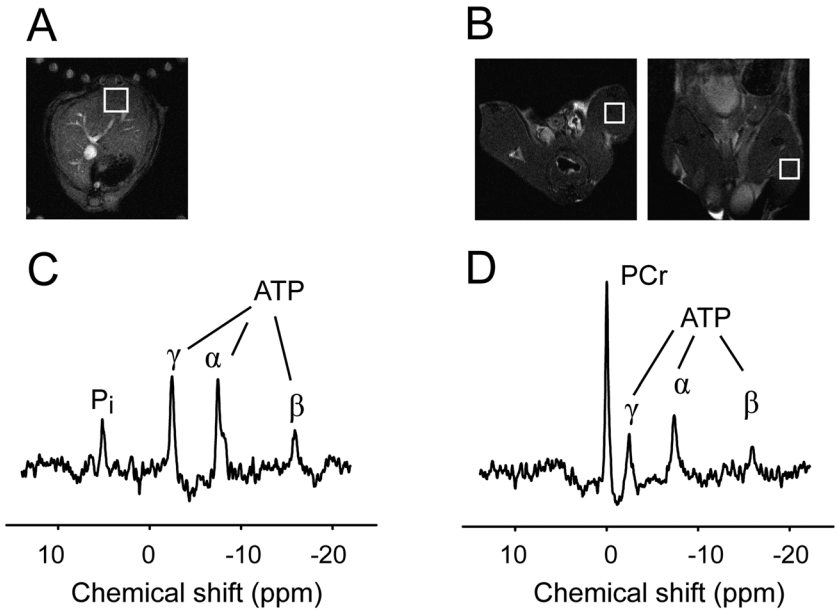

Figure 3. Voxel positioning for three-dimensional image-selected *in vivo* spectroscopy (3D ISIS) in (A) the liver ($5 \times 5 \times 5$ mm^3) and (B) hind limb skeletal muscle ($4 \times 4 \times 4$ mm^3) in the mouse, and the corresponding ^{31}P MR spectra for (C) the liver (NA = 768) and (D) skeletal muscle (NA = 384). Note the prominent resonance of PCr detected in skeletal muscle, whereas it is absent in liver tissue. α-, β-, γ-ATP, α-, β- and γ-phosphate groups in adenosine 5′-triphosphate; NA, number of averages; PCr, phosphocreatine; P_i, inorganic phosphate.

J-coupling constant of 17 Hz. The γ-ATP LWs ($LW_{\gamma\text{-ATP}}$) were constrained relative to the PCr LW (LW_{PCr}) according to an empirically determined relation: $LW_{\gamma\text{-ATP}} = LW_{PCr} + 14.85$ Hz ($n = 63$; $r = 0.78$; $P < 0.001$). Blood 2,3-diphosphoglycerate (2,3-DPG) resonances obscured the inorganic phosphate (P_i) resonance. Therefore, these signals were fitted with two peaks: one for 2,3-$DPG_{5.4\ ppm}$ and P_i at 5.4 ppm, and one for 2,3-$DPG_{6.3\ ppm}$ at 6.3 ppm.

Saturation recovery curves of PCr, γ-ATP and α-ATP were fitted by a mono-exponential function to estimate the corresponding longitudinal relaxation rate constants R_1. Mean R_1 values were used to determine metabolite T_1 values via $R_1 = 1/T_1$.

The *in vivo* myocardial energy status was expressed as the PCr/γ-ATP ratio, corrected for partial saturation.

Because blood contains ATP, but no PCr (24), signal contamination from blood in *in vivo* cardiac ^{31}P MR spectra may lead to the underestimation of the myocardial PCr/γ-ATP ratio. Therefore, we evaluated whether the PCr/γ-ATP ratio in the current work could be affected by blood contamination. The $[\gamma\text{-ATP}/2,3\text{-}DPG_{6.3\ ppm}]_{blood}$ ratio in spectra acquired in fresh blood was determined as a measure of the ATP content in blood. The contribution of resonances from blood metabolites to *in vivo* spectra was assessed by the quantification of the $[2,3\text{-}DPG_{6.3\ ppm}/\gamma\text{-ATP}]_{LV}$ ratio in the cardiac 3D ISIS spectra. Next, the relative contribution of signal from ATP in the blood to the ATP signal obtained with *in vivo* 3D ISIS was calculated as: $[\gamma\text{-ATP}/2,3\text{-}DPG_{6.3\ ppm}]_{blood} \times [2,3\text{-}DPG_{6.3\ ppm}/\gamma\text{-ATP}]_{LV} \times 100\%$.

Validations

To test our *in vivo* ^{31}P MRS method against conventional biochemical assays in *ex vivo* tissue samples, validation measurements were conducted in a separate cohort of healthy mice ($n = 4$). Following the acquisition of 3D ISIS-localized myocardial ^{31}P MR spectra as described above, the heart was immediately snap frozen on thoracotomy. Myocardial high-energy phosphate concentrations were determined spectrophotometrically as described previously (25).

To monitor the effects of anesthesia on hemodynamics and blood gases, healthy mice ($n = 5$) underwent cannulation of the carotid artery after the induction of isoflurane anesthesia. The mean arterial pressure (MAP) and heart rate were monitored using a heparinized saline-filled catheter connected to a blood pressure transducer (Baxter TruWave PX600F, Edwards, Irvine, CA, USA), and recorded using LabVIEW 5.1 (National Instruments, Austin, TX, USA), as described previously (26). Each experiment was continued for 1.5 h, and mimicked the experimental conditions of the *in vivo* ^{31}P MRS acquisitions in terms of mouse body temperature, heart and respiratory rates, and anesthesia maintenance, as described above. After 1.5 h, a 100-μL arterial blood sample was obtained via the cannula and subsequently analyzed using a blood gas analyzer (RAPIDPoint 500, Siemens Healthcare, Erlangen, Germany). Immediately thereafter, the anesthetized mice were sacrificed by snap freezing the heart on thoracotomy for *ex vivo* spectrophotometric assay of PCr and ATP concentrations (25).

Statistical analyses

Data are reported as the mean ± standard deviation (SD). The statistical significance of differences was analyzed using two-sided paired or unpaired *t*-tests, as appropriate. The level of significance was set at $P < 0.05$.

RESULTS

MRI: LV hypertrophy in TAC mice

We assessed the *in vivo* LV morphology and function from cine MR images to confirm the hypertrophic phenotype and impaired cardiac performance in TAC mice (Table 1, Fig. 1A, B). LV mass was 95% higher in TAC mice compared with healthy

Table 1. Left ventricle (LV) morphology and functional parameters obtained with MRI in control mice and transverse aortic constricted (TAC) mice

	Control (n = 9)	TAC (n = 8)	P
LV mass (mg)	90.0 ± 14.9	176 ± 19.1	***
LV mass/body weight (mg/g)	3.7 ± 0.6	6.0 ± 0.9	***
Heart rate (beats/min)	495 ± 50	539 ± 31	NS
End-diastolic volume (μL)	63.7 ± 10.8	123 ± 26.1	***
End-systolic volume (μL)	20.8 ± 5.4	94.1 ± 24.8	***
Stroke volume (μL)	43.0 ± 7.3	28.7 ± 6.6	***
Ejection fraction (%)	67.6 ± 5.6	23.9 ± 5.2	***

Data are expressed as mean ± standard deviation (SD). Effect of TAC (two-sided unpaired t-test):
***$P < 0.001$; NS, not significant.

mice ($P < 0.001$), indicating LV hypertrophy in TAC mice. Concomitantly, EDV ($P < 0.001$) and ESV ($P < 0.001$) were higher in TAC mice compared with controls. This translated into a lower SV (–33%, $P < 0.001$) and EF (–65%, $P < 0.001$) in TAC mice. Combined, these data illustrate the development of dilated hypertrophic cardiomyopathy with severe systolic dysfunction after 7 weeks of LV pressure overload in TAC mice.

^{31}P MRS: *in vivo* myocardial energy status

Typical ^{31}P MR spectra acquired with 3D ISIS in a healthy mouse heart and a TAC heart are shown in Fig. 1C, D. Resonances of PCr and ATP are indicated. Inorganic phosphate (P_i, ~5 ppm) was obscured by 2,3-DPG arising from blood. The spectral LW for PCr was 0.37 ± 0.15 ppm.

Conventional pulse-acquire ^{31}P MR saturation recovery experiments of the mouse chest were performed in order to estimate the high-energy phosphate metabolite T_1 relaxation times at 9.4 T. T_1 values did not differ between control mice and TAC mice, and were 2.54 ± 0.41 s for PCr, 1.45 ± 0.25 s for γ-ATP and 1.09 ± 0.31 s for α-ATP. Given TR = 2 s, this resulted in a partial saturation correction factor for PCr/γ-ATP of 1.37 in 3D ISIS experiments. In healthy mice (n = 6), 3D ISIS was also performed under fully relaxed conditions. These localized acquisitions yielded a partial saturation correction factor for myocardial PCr/γ-ATP of 1.38 ± 0.28 for spectra acquired at TR = 2 s, which is in good agreement with the value derived from the unlocalized pulse-acquire saturation recovery experiments. Myocardial PCr/γ-ATP, corrected for partial saturation, was lower in TAC mice compared with healthy controls (0.76 ± 0.13 *versus* 1.00 ± 0.15; $P < 0.01$, Fig. 1E), which is indicative of a compromised myocardial energy homeostasis in TAC mice.

Localization of a slice containing anterior myocardial wall with 1D ISIS (Fig. 2A) systematically resulted in higher PCr/γ-ATP ratios than those obtained with 3D ISIS of the whole LV (2.12 ± 0.61 *versus* 1.08 ± 0.25; $P < 0.01$, Fig. 2G). Skeletal muscle tissue surrounding the anterior myocardial wall within the sensitive area of the surface coil (Fig. 2A) probably contributed to the higher PCr/γ-ATP ratio observed with 1D ISIS. This was corroborated by spectra (Fig. 2E) obtained with a very small 9-μL 3D ISIS voxel positioned in the anterior myocardial wall (Fig. 2B), which qualitatively confirm the PCr/γ-ATP ratio of approximately unity for healthy myocardium.

^{31}P MRS of liver, skeletal muscle and blood

Using the respiratory-gated and cardiac-triggered 3D ISIS approach, we acquired ^{31}P MR spectra from *in vivo* mouse liver and hind limb skeletal muscle. The absence of PCr in liver tissue was confirmed (Fig. 3C), illustrating that essentially no signal from PCr in adjacent skeletal muscle contaminated the spectra that were obtained from the liver with 3D ISIS. Spectra obtained from hind limb skeletal muscle yielded a PCr/γ-ATP ratio of 3.59 ± 0.58 (Fig. 3D), which is typical of healthy mouse skeletal muscle in resting conditions (21,27).

In spectra obtained from fresh blood (Fig. 4), the blood ATP content was estimated via the $[\gamma\text{-ATP}/2,3\text{-DPG}_{6.3\ ppm}]_{blood}$ ratio, which was 0.22 ± 0.14. The contribution of signal from metabolites in the blood to the cardiac spectra, estimated via $[2,3\text{-DPG}_{6.3\ ppm}/\gamma\text{-ATP}]_{LV}$, was similar for controls and TAC mice, and was 0.18 ± 0.10. The relative contribution of signal from ATP in the blood to the ATP signal in cardiac 3D ISIS spectra was therefore approximately 4%. These results show that contamination of the 3D ISIS spectra with signal from ATP in LV blood is marginal, and only minimally affects the myocardial PCr/γ-ATP ratio.

Validations

The *in vivo* PCr/γ-ATP ratio measured with 3D ISIS-localized ^{31}P MRS in healthy control mice (1.00 ± 0.19; n = 19) matched conventional *ex vivo* spectrophotometric assays in myocardial tissue (0.94 ± 0.24; n = 8; Fig. 5A). In a subset of healthy mice, both *in vivo* and *ex vivo* measurements were performed. Spectrophotometric assays in myocardial tissue mirrored *in vivo* ^{31}P MRS measurements of myocardial PCr/γ-ATP ratios in the same hearts (1.00 ± 0.32 *versus* 0.94 ± 0.14; n = 4; Fig. 5B). Concentrations of PCr and ATP in *ex vivo* myocardial tissue samples (n = 8) were 18.3 ± 5.7 mmol/kg dry weight and 19.3 ± 2.5 mmol/kg dry weight, respectively.

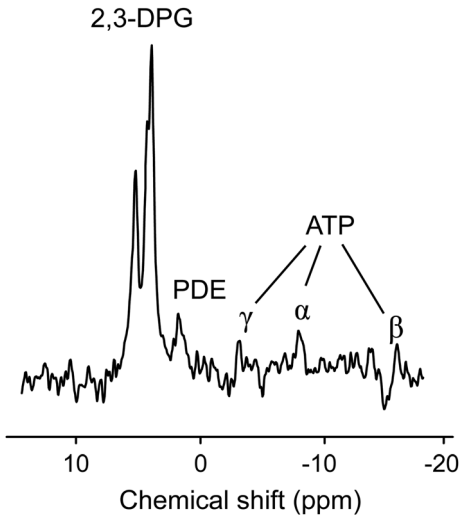

Figure 4. ^{31}P MR spectrum obtained from fresh blood. α-, β-, γ-ATP, α-, β- and γ-phosphate groups in adenosine 5′-triphosphate; 2,3-DPG, 2,3-diphosphoglycerate; PDE, phosphodiesters.

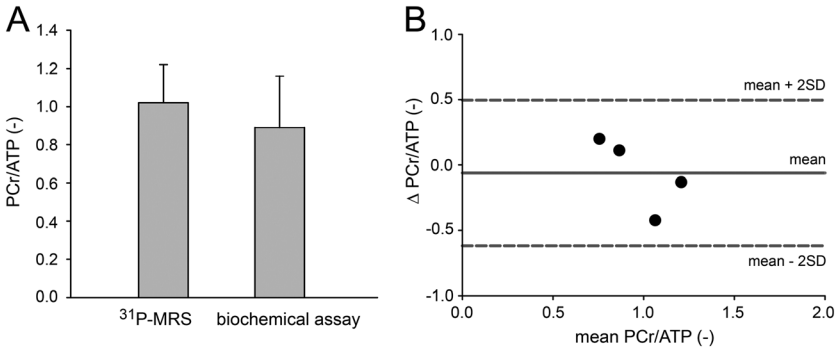

Figure 5. (A) Comparison of *in vivo* three-dimensional image-selected *in vivo* spectroscopy (3D ISIS)-localized ^{31}P MRS measurements (n = 19) and conventional *ex vivo* spectrophotometric assays (n = 8) of the myocardial PCr/ATP ratio in healthy mice. Data are expressed as mean ± standard deviation (SD). In a subset of healthy mice (n = 4), both ^{31}P MRS and biochemical assays were performed. The difference in PCr/ATP ratio between the two methods is plotted against the mean per mouse in a Bland–Altman plot (B). Broken lines indicate the limits of agreement (mean ± 2SD) around the mean (full line). ATP, adenosine 5′-triphosphate; PCr, phosphocreatine.

Mouse hemodynamics and blood gases were measured after 1.5 h of anesthesia to assess the potential effects of the isoflurane anesthetic regimen on the cardiovascular physiology. Throughout these experiments, which mimicked the experimental conditions of the ^{31}P MRS procedure, MAP (90 ± 3.3 mmHg) and heart rate (497 ± 76 beats/min) remained well within the physiological range for healthy C57BL/6 mice (28). Moreover, after 1.5 h of anesthesia, blood oxygen saturation and other blood gas parameters were normal (Table 2). These data illustrate that the experimental conditions of the *in vivo* MR protocol have no major influence on mouse hemodynamics or blood gases.

DISCUSSION

We have described a non-invasive method to study the *in vivo* myocardial energy status in healthy and diseased mice using 3D ISIS-localized ^{31}P MRS. Acquisitions were respiratory gated and cardiac triggered, whilst maintaining steady-state conditions using dummy excitations to ensure accurate localization. We validated our method against conventional biochemical assays of PCr and ATP concentrations in *ex vivo* myocardial tissue collected immediately after the acquisition of the *in vivo* ^{31}P MR spectra. Using a ^{1}H/^{31}P MR set-up, cardiac ^{31}P MRS with 3D ISIS was combined with cine ^{1}H MRI to assess morphological, functional and metabolic parameters in a single experimental session of less than 2 h. With this approach, we identified a reduced myocardial energy status, evidenced by a ~25% lower PCr/γ-ATP ratio, accompanied by hypertrophic growth and severely impaired myocardial function in a surgical mouse model of heart failure. These pathophysiological changes are consistent with previous studies (16,29).

Table 2. Hemodynamics and blood gases measured in control mice after 1.5 h of anesthesia (1.2–1.6% isoflurane in a continuous flow of 0.4 L/min of medical air)

	C57BL/6 (n = 5)
Heart rate (beats/min)	497 ± 76
Mean arterial pressure (mmHg)	90 ± 3.3
pH	7.41 ± 0.03
pCO_2 (mmHg)	31.6 ± 3.5
pO_2 (mmHg)	110.7 ± 4.4
Total hemoglobin (mM)	9.2 ± 0.2
O_2 saturation (%)	96.2 ± 0.6

Data are expressed as mean ± standard deviation (SD).

The myocardial PCr/ATP ratio in healthy mice was approximately unity, measured both *in vivo* with ^{31}P MRS and *ex vivo* with spectrophotometric assays in the same hearts. This value is on the lower range of the normal PCr/ATP values reported in the literature for humans (overall mean, 1.72 ± 0.26) (30). In humans, heart rate and cardiac work can increase up to threefold during dobutamine stress (31) or exercise (32). In healthy mice, dobutamine infusion induced a heart rate increase of only approximately 39% (27), whereas running exercise increased mouse heart rates by only 40–90% (33,34). Indeed, it has been suggested that mice may have a lower cardiac energy reserve (35), given the narrower dynamic range of heart rates and cardiac work in mice relative to humans.

Notably, the myocardial PCr/ATP ratio for healthy mice in the current work was lower than the PCr/ATP values obtained in other *in vivo* ^{31}P MRS mouse studies (9–11). From measurements of the physiological hemodynamics and blood gases during 1.5 h of anesthesia (28,36), we ruled out any adverse effects of the experimental conditions on mouse cardiovascular physiology that may cause a decreased PCr/ATP ratio. Instead, many technical aspects of localized ^{31}P MRS acquisition and quantification could contribute to the variability in the MRS-derived PCr/ATP values reported in the literature (30), and should be taken into consideration when comparing between different laboratories (37,38). The three main causes of the apparent discrepancies in literature reports are differences in: (i) correction for partial saturation; (ii) contamination of the spectra by signal from the liver or skeletal muscle tissue; and (iii) contaminating blood in the LV cavity (30). Below, each of these issues is addressed for the current study.

Partial saturation correction

For the correction of partial saturation effects, we used metabolite T_1 values as determined by unlocalized pulse-acquire saturation recovery experiments. Because the T_1 values in chest skeletal muscle could be different from those in cardiac muscle (39), we validated the correction factor in healthy mice by acquiring 3D ISIS-localized spectra from the LV myocardium under fully relaxed conditions. Indeed, the partial saturation correction

factor derived from unlocalized saturation recovery experiments was in agreement with measurements localized to the heart. This observation validates the assumption (40) that, in the healthy mouse, the T_1(PCr)/T_1(γ-ATP) ratio is essentially the same for chest skeletal muscle and myocardium at 9.4 T (11).

Minimization of signal contamination

Because 3D ISIS requires multiple acquisitions for signal localization, the method is particularly sensitive to motion artifacts and consequential contamination from tissues surrounding the heart, such as the liver and chest skeletal muscle. Additional contamination ('T_1 smearing') can be introduced by differences in longitudinal magnetization between subsequent acquisitions within one ISIS cycle as a result of the imperfect flip angle of the excitation pulse combined with a TR $< 5 \times T_1$ (12,13,19). Similar effects occur when TR is not constant between acquisitions, whilst measuring at TR $< 5 \times T_1$. Previous studies in rodents (9) and humans (41–43) using 3D ISIS for cardiac applications did not measure at constant TR for steady-state magnetization, or at fully relaxed conditions. The 3D ISIS sequence presented here uses a respiratory-gated and cardiac-triggered timing strategy to ensure localized inversion of the LV signal at identical cardiac and respiratory phases for all acquisitions, in combination with dummy excitations during respiratory gates to maintain a constant TR. In addition, by using the γ-ATP signal to determine the PCr/ATP ratio, we minimized the chemical shift displacement between PCr and ATP. The PCr signal was absent in 3D ISIS-localized liver spectra, demonstrating that skeletal muscle located between the surface coil and the voxel of interest did not contaminate the spectra and that signal acquisition was effectively restricted to the liver. Indeed, localized ^{31}P MRS of the liver (20) will also benefit from the strategy proposed here (44).

Moreover, we demonstrated the effect of potential contamination of the spectra with signal from chest skeletal muscle by comparing 3D ISIS of the whole LV with 1D ISIS of a slice containing the anterior myocardial wall, similar to 1D CSI approaches reported previously (10,45). Localization within the selected slice is realized by surface coil positioning (Fig. 2A), which may introduce signal from the surrounding tissue to the resultant spectrum. The PCr/γ-ATP ratio obtained with 1D ISIS was consistent with values observed with 1D CSI (10), but two-fold higher than the myocardial PCr/γ-ATP ratio measured with 3D ISIS.

Blood contamination

Blood in the LV cavity contains ATP, but no PCr. If signal from ATP in the blood contributes to the signal acquired from the voxel of interest, the myocardial PCr/ATP ratio may be underestimated (46). A correction factor can be applied to account for signal contribution from ATP in the blood to the spectra, which depends on both the amount of ATP in the blood and the amount of blood contributing to the spectrum. We showed that the amount of ATP signal from fresh blood, in terms of $[\gamma\text{-ATP}/2,3\text{-DPG}_{6.3\ ppm}]_{blood}$, was approximately 20%, which is consistent with previous reports of ^{31}P MRS studies of blood in humans (24) and mice (9,47). The contribution of signal from metabolites in blood to the *in vivo* 3D ISIS spectra of the whole LV, estimated via $[2,3\text{-DPG}_{6.3\ ppm}/\gamma\text{-ATP}]_{LV}$, was less than 20%, and was not different between healthy and TAC mice. The high velocity of flowing blood during the acquisition may attenuate the peaks from blood metabolites in spectra obtained *in vivo* (48). Based on these observations, we estimated that the contribution of signal from ATP in the blood to the ATP signal in *in vivo* 3D ISIS spectra was only 4%, and concluded that correcting for blood contamination was not necessary in this study. Moreover, spectra obtained with 3D ISIS selecting a small voxel confined to the anterior myocardial wall were similar to those obtained from the whole LV, confirming the minimal contribution of signal from blood to the latter.

Study limitations

With our current approach of determining the PCr/ATP ratio, it is not possible to detect similar decreases in both PCr and ATP concentrations. The absolute quantification of metabolite concentration will therefore be more sensitive to changes in cardiac energy metabolism. Indeed, it has been shown that, in pressure-overload mouse hearts, not only do myocardial PCr levels drop, but also ATP concentrations decrease, illustrating the added value of absolute quantification over the PCr/ATP ratio (45,49). Nonetheless, the PCr/ATP ratio has been used to identify perturbations in myocardial energy homeostasis in various mouse models of disease (16,50,51). Furthermore, a reduced PCr/ATP ratio has been shown to be an important indicator of disease severity (16).

A drawback of using single-voxel-localized ^{31}P MRS of the entire LV is that myocardial energy status cannot be assessed at a regional scale, which is of importance in investigations of myocardial ischemia. *In vivo* 2D ^{31}P CSI of the mouse heart (11) would allow for the mapping of myocardial energetics to assess differences between infarcted and remote regions in mouse models of myocardial ischemic insult. Nonetheless, because many preclinical animal studies focus on pathologies that have a global effect on the heart, such as aortic stenosis, diabetes and inborn errors of metabolism, the current 3D ISIS approach for localized ^{31}P MRS can be a valuable addition to the toolbox of mouse cardiac MR methods (4).

Even at the high magnetic field strength of 9.4 T, we were unable to unambiguously detect and quantify myocardial P_i, because the signal was obscured by signal from 2,3-DPG in the blood. Potentially, reliable detection of P_i would provide additional metabolic insights, as decreasing PCr levels may be mirrored by increasing P_i levels. In addition, the chemical shift of P_i could potentially be used to quantify *in vivo* myocardial pH. Notably, even in the human heart, P_i is often undetectable, suggesting that myocardial P_i may only be partially MR visible (30).

CONCLUSIONS

The present work describes a non-invasive approach to assess myocardial energy status in the *in vivo* mouse using single-voxel 3D ISIS-localized ^{31}P MRS, which was validated by conventional biochemical assays in *ex vivo* myocardial tissue samples from the same hearts. The method encompasses a respiratory-gated, cardiac-triggered 3D ISIS sequence, with dummy excitations during respiratory gates, to ensure a well-defined localization. This method identified differences in high-energy phosphate metabolism between the healthy mouse heart and a widely used model for heart failure, the TAC mouse. Importantly, results were obtained under physiological conditions, which are difficult or impossible to achieve with disruptive methods, such as open-thorax protocols or isolated perfused heart set-ups. Furthermore, the 3D ISIS-localized spectra can be obtained within 40 min, leaving room for

measurements of cardiac function with MRI during the same experimental session. We anticipate that localized ^{31}P MRS will provide valuable contributions to preclinical investigations of cardiac disease progression and therapeutic intervention efficacy.

Acknowledgements

We thank Larry de Graaf and Tom R. Geraedts for the design of dedicated hardware, Esther C. M. Kneepkens for contributions to pulse sequence design and Leonie B. P. Niesen for biotechnical assistance. Dr Jeroen A. L. Jeneson is acknowledged for helpful discussions.

This work was supported by the Center for Translational Molecular Medicine, project TRIUMPH (grant number 01C-103), with funding from the Dutch Heart Foundation. S.M.H. and J.J.P. are supported by VIDI grants (project numbers 016.086.336 and 700.58.421, respectively) from the Netherlands Organization for Scientific Research (NWO). Part of this work was supported by the National Institutes of Health (NIH) (A.J.B. and G.J.S.; NIH grant HL072011).

REFERENCES

1. Neubauer S. The failing heart – an engine out of fuel. N. Engl. J. Med. 2007; 356: 1140–1151.
2. Epstein FH. MR in mouse models of cardiac disease. NMR Biomed. 2007; 20: 238–255.
3. Kober F, Troalen T, Bernard M. Recent developments in small animal cardiovascular MRI. Curr. Cardiovasc. Imaging Rep. 2014; 7: 9249.
4. Bakermans AJ, Abdurrachim D, Moonen RPM, Motaal AG, Prompers JJ, Strijkers GJ, Vandoorne K, Nicolay K. Small animal cardiovascular MR imaging and spectroscopy. Prog. Nucl. Magn. Reson. Spectrosc. 2015; 88-89: 1–47.
5. Weiss RG, Bottomley PA, Hardy CJ, Gerstenblith G. Regional myocardial metabolism of high-energy phosphates during isometric exercise in patients with coronary artery disease. N. Engl. J. Med. 1990; 323: 1593–1600.
6. Keevil SF. Spatial localization in nuclear magnetic resonance spectroscopy. Phys. Med. Biol. 2006; 51: R579–R636.
7. Ordidge RJ, Connelly A, Lohman JA. Image-selected in vivo spectroscopy (ISIS). A new technique for spatially selective NMR spectroscopy. J. Magn. Reson. 1986; 66: 283–294.
8. de Graaf RA. *In Vivo NMR Spectroscopy: Principles and Techniques*. John Wiley & Sons: Chichester; 2007.
9. Omerovic E, Basetti M, Bollano E, Bohlooly-Y M, Bohlooly M, Törnell J, Isgaard J, Hjalmarson A, Soussi B, Waagstein F. In vivo metabolic imaging of cardiac bioenergetics in transgenic mice. Biochem. Biophys. Res. Commun. 2000; 271: 222–228.
10. Chacko VP, Aresta F, Chacko SM, Weiss RG. MRI/MRS assessment of in vivo murine cardiac metabolism, morphology, and function at physiological heart rates. Am. J. Physiol. Heart Circ. Physiol. 2000; 279: H2218–H2224.
11. Flögel U, Jacoby C, Gödecke A, Schrader J. In vivo 2D mapping of impaired murine cardiac energetics in NO-induced heart failure. Magn. Reson. Med. 2007; 57: 50–58.
12. Lawry TJ, Karczmar GS, Weiner MW, Matson GB. Computer simulation of MRS localization techniques: an analysis of ISIS. Magn. Reson. Med. 1989; 9: 299–314.
13. Keevil SF, Porter DA, Smith MA. Experimental characterization of the ISIS technique for volume selected NMR spectroscopy. NMR Biomed. 1992; 5: 200–208.
14. Bakermans AJ, Abdurrachim D, Geraedts TR, Houten SM, Nicolay K, Prompers JJ. In vivo proton T_1 relaxation times of mouse myocardial metabolites at 9.4 T. Magn. Reson. Med. 2015; 73: 2069–2074.
15. Rockman HA, Ross RS, Harris AN, Knowlton KU, Steinhelper ME, Field LJ, Ross J, Chien KR. Segregation of atrial-specific and inducible expression of an atrial natriuretic factor transgene in an in vivo murine model of cardiac hypertrophy. Proc. Natl. Acad. Sci. U. S. A., 1991; 88: 8277–8281.
16. Maslov MY, Chacko VP, Stuber M, Moens AL, Kass DA, Champion HC, Weiss RG. Altered high-energy phosphate metabolism predicts contractile dysfunction and subsequent ventricular remodeling in pressure-overload hypertrophy mice. Am. J. Physiol. Heart Circ. Physiol. 2007; 292: H387–H391.
17. van Nierop BJ, van Assen HC, van Deel ED, Niesen LBP, Duncker DJ, Strijkers GJ, Nicolay K. Phenotyping of left and right ventricular function in mouse models of compensated hypertrophy and heart failure with cardiac MRI. PLoS One, 2013; 8: e55424.
18. Bakermans AJ, Geraedts TR, van Weeghel M, Denis S, João Ferraz M, Aerts JMFG, Aten J, Nicolay K, Houten SM, Prompers JJ. Fasting-induced myocardial lipid accumulation in long-chain acyl-CoA dehydrogenase knockout mice is accompanied by impaired left ventricular function. Circ. Cardiovasc. Imaging, 2011; 4: 558–565.
19. Burger C, Buchli R, McKinnon G, Meier D, Boesiger P. The impact of the ISIS experiment order on spatial contamination. Magn. Reson. Med. 1992; 26: 218–230.
20. Landis CS, Yamanouchi K, Zhou H, Mohan S, Roy-Chowdhury N, Shafritz DA, Koretsky A, Roy-Chowdhury J, Hetherington HP, Guha C. Noninvasive evaluation of liver repopulation by transplanted hepatocytes using ^{31}P MRS imaging in mice. Hepatology, 2006; 44: 1250–1258.
21. Kan HE, Veltien A, Arnts H, Nabuurs CIHC, Luijten B, de Haan A, Wieringa B, Heerschap A. Gated dynamic ^{31}P MRS shows reduced contractile phosphocreatine breakdown in mice deficient in cytosolic creatine kinase and adenylate kinase. NMR Biomed. 2009; 22: 523–531.
22. Heijman E, Aben J-P, Penners C, Niessen P, Guillaume R, van Eys G, Nicolay K, Strijkers GJ. Evaluation of manual and automatic segmentation of the mouse heart from CINE MR images. J. Magn. Reson. Imaging, 2008; 27: 86–93.
23. Vanhamme L, van den Boogaart A, van Huffel S. Improved method for accurate and efficient quantification of MRS data with use of prior knowledge. J. Magn. Reson. 1997; 129: 35–43.
24. Horn M, Neubauer S, Bomhard M, Kadgien M, Schnackerz K, Ertl G. ^{31}P-NMR spectroscopy of human blood and serum: first results from volunteers and patients with congestive heart failure, diabetes mellitus and hyperlipidaemia. MAGMA Magn. Reson. Mater. Phys. Biol. Med. 1993; 1: 55–60.
25. Lamprecht W, Trautschold I. ATP determination, with hexokinase and glucose-6-phosphate dehydrogenase. In: Bergmeyer HU (ed.). *Methods of Enzymatic Analysis*. Academic Press: New York; 1974, pp. 2101–2110.
26. Zuurbier CJ, Koeman A, Houten SM, Hollmann MW, Florijn WJ. Optimizing anesthetic regimen for surgery in mice through minimization of hemodynamic, metabolic, and inflammatory perturbations. Exp. Biol. Med. (Maywood), 2014; 239: 737–746.
27. Naumova AV, Weiss RG, Chacko VP. Regulation of murine myocardial energy metabolism during adrenergic stress studied by in vivo ^{31}P NMR spectroscopy. Am. J. Physiol. Heart Circ. Physiol. 2003; 285: H1976–H1979.
28. Constantinides C, Mean R, Janssen BJ. Effects of isoflurane anesthesia on the cardiovascular function of the C57BL/6 mouse. ILAR Journal 2011; 52: e21–e31.
29. Gupta A, Chacko VP, Schär M, Akki A, Weiss RG. Impaired ATP kinetics in failing in vivo mouse heart. Circ. Cardiovasc. Imaging, 2011; 4: 42–50.
30. Bottomley PA. NMR spectroscopy of the human heart. In: Harris RK, Wasylishen RE, eds. *Encyclopedia of Magnetic Resonance*. John Wiley & Sons: Chichester; 2009. DOI: 10.1002/9780470034590.emrstm0345.pub2
31. Lamb HJ, Beyerbacht HP, Ouwerkerk R, Doornbos J, Pluim BM, van der Wall EE, van der Laarse A, de Roos A. Metabolic response of normal human myocardium to high-dose atropine–dobutamine stress studied by ^{31}P-MRS. Circulation, 1997; 96: 2969–2977.
32. La Gerche A, Claessen G, van de Bruaene A, Pattyn N, van Cleemput J, Gewillig M, Bogaert J, Dymarkowski S, Claus P, Heidbuchel H. Cardiac MRI: a new gold standard for ventricular volume quantification during high-intensity exercise. Circ. Cardiovasc. Imaging, 2013; 6: 329–338.
33. Adlam D, de Bono JP, Danson EJ, Zhang MH, Casadei B, Paterson DJ, Channon KM. Telemetric analysis of haemodynamic regulation during voluntary exercise training in mouse models. Exp. Physiol. 2011; 96: 1118–1128.
34. Lujan HL, Janbaih H, Feng H-Z, Jin J-P, DiCarlo SE. Ventricular function during exercise in mice and rats. Am. J. Physiol. Regul. Integr. Comp. Physiol. 2012; 302: R68–R74.
35. Saupe KW, Spindler M, Tian R, Ingwall JS. Impaired cardiac energetics in mice lacking muscle-specific isoenzymes of creatine kinase. Circ. Res. 1998; 82: 898–907.
36. Schwarzkopf TM, Horn T, Lang D, Klein J. Blood gases and energy metabolites in mouse blood before and after cerebral ischemia: the effects of anesthetics. Exp. Biol. Med. (Maywood), 2013; 238: 84–89.

37. Bottomley PA. The trouble with spectroscopy papers. Radiology, 1991; 181: 344–350.
38. Lamb HJ, Doornbos J, den Hollander JA, Luyten PR, Beyerbacht HP, van der Wall EE, de Roos A. Reproducibility of human cardiac ^{31}P-NMR spectroscopy. NMR Biomed. 1996; 9: 217–227.
39. van Dobbenburgh JO, Lekkerkerk C, van Echteld CJ, de Beer R. Saturation correction in human cardiac ^{31}P MR spectroscopy at 1.5 T. NMR Biomed. 1994; 7: 218–224.
40. Bottomley PA, Hardy CJ, Weiss RG. Correcting human heart ^{31}P NMR spectra for partial saturation. Evidence that saturation factors for PCr/ATP are homogeneous in normal and disease states. J. Magn. Reson. 1991; 95: 341–355.
41. Schaefer S, Gober J, Valenza M, Karczmar GS, Matson GB, Camacho SA, Botvinick EH, Massie B, Weiner MW. Nuclear magnetic resonance imaging-guided phosphorus-31 spectroscopy of the human heart. J. Am. Coll. Cardiol. 1988; 12: 1449–1455.
42. van der Meer RW, Hammer S, Smit JWA, Frölich M, Bax JJ, Diamant M, Rijzewijk LJ, de Roos A, Romijn JA, Lamb HJ. Short-term caloric restriction induces accumulation of myocardial triglycerides and decreases left ventricular diastolic function in healthy subjects. Diabetes, 2007; 56: 2849–2853.
43. Fragasso G, de Cobelli F, Spoladore R, Esposito A, Salerno A, Calori G, Montanaro C, Maranta F, Lattuada G, Margonato A, Del Maschio A, Perseghin G. Resting cardiac energy metabolism is inversely associated with heart rate in healthy young adult men. Am. Heart J. 2011; 162: 136–141.
44. Solanky BS, Sanchez-Canon GJ, Cobbold JFL, Taylor-Robinson SD, Bell JD, Scudamore CL, Ross E, Holder JC, So P-W, Cox IJ. Metabolic profiling of the rat liver after chronic ingestion of alpha-naphthylisothiocyanate using in vivo and ex vivo magnetic resonance spectroscopy. Toxicol. Sci. 2012; 126: 306–316.
45. Gupta A, Chacko VP, Weiss RG. Abnormal energetics and ATP depletion in pressure-overload mouse hearts: in vivo high-energy phosphate concentration measures by noninvasive magnetic resonance. Am. J. Physiol. Heart Circ. Physiol. 2009; 297: H59–H64.
46. Hardy CJ, Weiss RG, Bottomley PA, Gerstenblith G. Altered myocardial high-energy phosphate metabolites in patients with dilated cardiomyopathy. Am. Heart J. 1991; 122: 795–801.
47. Lee J, Hu Q, Nakamura Y, Wang X, Zhang X, Zhu X, Chen W, Yang Q, Zhang J. Open-chest ^{31}P magnetic resonance spectroscopy of mouse heart at 4.7 Tesla. J. Magn. Reson. Imaging, 2006; 24: 1269–1276.
48. Zhang J, Duncker DJ, Xu Y, Zhang Y, Path G, Merkle H, Hendrich K, From AH, Bache RJ, Uğurbil K. Transmural bioenergetic responses of normal myocardium to high workstates. Am. J. Physiol. 1995; 268: H1891–H1905.
49. Gupta A, Akki A, Wang Y, Leppo MK, Chacko VP, Foster DB, Caceres V, Shi S, Kirk JA, Su J, Lai S, Paolocci N, Steenbergen C, Gerstenblith G, Weiss RG. Creatine kinase-mediated improvement of function in failing mouse hearts provides causal evidence the failing heart is energy starved. J. Clin. Invest. 2012; 122: 291–302.
50. Bakermans AJ, Dodd MS, Nicolay K, Prompers JJ, Tyler DJ, Houten SM. Myocardial energy shortage and unmet anaplerotic needs in the fasted long-chain acyl-CoA dehydrogenase knockout mouse. Cardiovasc. Res. 2013; 100: 441–449.
51. Tucci S, Flögel U, Hermann S, Sturm M, Schäfers M, Spiekerkoetter U. Development and pathomechanisms of cardiomyopathy in very long-chain acyl-CoA dehydrogenase deficient (VLCAD(–/–)) mice. Biochim. Biophys. Acta, 2014; 1842: 677–685.